J Atmos Chem (2006) 55:147–166
DOI 10.1007/s10874-006-9033-y

ORIGINAL ARTICLE

Measurement and investigation of chamber radical sources in the European Photoreactor (EUPHORE)

Judit Zádor · Tamás Turányi · Klaus Wirtz · Michael J. Pilling

Received: 17 December 2005 / Accepted: 24 May 2006

Abstract It is essential to quantify the background reactivity of smog-chambers, since this might be the major limitation of experiments carried out at low pollutant concentrations typical of the polluted atmosphere. Detailed investigation of three chamber experiments at zero-NO_x in the European Photoreactor (EUPHORE) were carried out by means of rate-of-production analysis and two uncertainty analysis tools: local uncertainty analysis and Monte Carlo simulations with Latin hypercube sampling. The chemical mechanism employed was that for methane plus the inorganic subset of the Master Chemical Mechanism (MCMv3.1). Newly installed instruments in EUPHORE allowed the measurement of nitrous acid and formaldehyde at sub-ppb concentrations with high sensitivity. The presence of HONO and HCHO during the experiments could be explained only by processes taking place on the FEP Teflon walls. The HONO production rate can be described by the empirical equation $W(\mathrm{HONO})^{\mathrm{dry}}_{\mathrm{EUPHORE}} = a \times j_{\mathrm{NO_2}} \times \exp(-T_0/T)$ in the low relative humidity region ($RH < 2\%$, $a = 7.3 \times 10^{21}\,\mathrm{cm}^{-3}$, $T_0 = 8945\,\mathrm{K}$), and by the equation $W(\mathrm{HONO})^{\mathrm{humid}}_{\mathrm{EUPHORE}} = W(\mathrm{HONO})^{\mathrm{dry}}_{\mathrm{EUPHORE}} + j_{\mathrm{NO_2}} \times b \times RH^q$ in the higher relative humidity region ($2\% < RH < 15\%, b = 5.8 \times 10^8\,\mathrm{cm}^{-3}$ and $q = 0.36$, and RH is the relative humidity in percentages). For HCHO the expression $W(\mathrm{HCHO})_{\mathrm{EUPHORE}} = c \times j_{\mathrm{NO_2}} \exp(-T_0'/T)$ is applicable ($c = 3.1 \times 10^{17}\,\mathrm{cm}^{-3}$ and $T_0' = 5686\,\mathrm{K}$). In the 0–15% relative humidity range OH production from HONO generated at the wall is about a factor of two higher than that from the photolysis of 100 ppb ozone. Effect of added NO_2 was found to be consistent with the dark HONO formation rate coefficient of MCMv3.1.

J. Zádor (✉) · T. Turányi
Department of Physical Chemistry, Eötvös University (ELTE), H-1117 Budapest, Pázmány P. stny. 1/A, Budapest, Hungary
e-mail: zador@chem.elte.hu

K. Wirtz
Centro de Estudios Ambientales del Mediterraneo (CEAM), Valencia, Spain

M. J. Pilling
Department of Chemistry, University of Leeds, Leeds, U.K.

Keywords European Photoreactor · Master Chemical Mechanism · Radical sources · Smog chamber · Uncertainty analysis · Formaldehyde · Nitrous acid

1. Introduction

Smog chambers are extensively used to test and develop tropospheric chemical kinetic mechanisms. One of their most important limitations is the wall effect. The heterogeneous chemistry taking place on the walls of the chamber alters the chemical composition of the gas-phase and therefore necessitates determination and use of a heterogeneous chamber mechanism. Although evidence for the existence of these reactions has been established for a long time (e.g. Carter *et al.*, 1981; Carter *et al.*, 1982; Carter and Lurmann, 1991; Killus and Whitten, 1990; Jeffries *et al.*, 2000), our knowledge is still imperfect in this area, partly because of the variability between the various chambers. However, improvements in analytical techniques (e.g. Heland *et al.*, 2001) and an improved knowledge of gas-phase elementary reaction rates and mechanisms now allows improved quantification of chamber processes, as it was done by Rohrer *et al.* (2005).

The most comprehensive listing of possible wall reactions may be found in the work of Carter and Lurmann (1991). These reactions are (i) dark hydrolysis of NO_2 on the walls producing HONO, (ii) photo-induced HONO production from NO_2, (iii) a photo-induced NO_x off-gassing process, (iv) N_2O_5 hydrolysis on the walls, (v) dark O_3 loss on the walls and (vi) off-gassing of organic compounds. The processes involving NO_y species imply a complex mechanism, which is not yet well understood. Probably the dark hydrolysis of NO_2 is the only one for which recent studies have yielded comprehensive knowledge (Pitts *et al.*, 1984; Finlayson-Pitts *et al.*, 2003; Rivera-Figueroa *et al.*, 2003). However, this reaction seems to be slower in FEP Teflon chambers than photo-induced HONO formation, for which under acidic conditions, a detailed mechanism was proposed by Zhou *et al.* (2002).

Another important general observation (Carter *et al.*, 1982; Glasson and Dunker, 1989) is that the usual NO_x/VOC experiments can be interpreted on the basis of two types of wall radical sources only. It was shown by Carter *et al.* (1982) that the use of one type of source does not give appropriate results, but taking into account both is satisfactory. There is an initial radical source, which is most likely due to the presence of some initial HONO, possibly from the impurities of the initial NO_x. Because of the short lifetime of HONO, it is important only in the first half an hour of a typical VOC–NO_x chamber experiment. It has been shown (see Bloss *et al.*, 2005) that, other than acting as a source of radicals in the very early stages, up to 1.5 ppb of initial HONO did not have any significant effect on ethene–NO_x experiments lasting 5–6 h on average. The other source discussed by Carter *et al.* (1982) is a continuous one, influencing the system on longer timescales. It is most probably due to the above mentioned wall reactions.

The main aim of this paper is the determination of rates of production of gas phase species in the European Photoreactor (EUPHORE) that can act as radical sources at the chamber wall, via a detailed analysis of experimental results. The rate parameters obtained are also backed with uncertainty information arising from the uncertainties of the applied chemical kinetic model. Our aims did not include giving a mechanistic explanation for the observed production rates, although some aspects will be considered. In the first part of the paper, the experimental conditions and the applied chemical mechanism are described. It is followed by the determination of the mean values of the production rates from wall reactions. In the subsequent section, the uncertainty sources and their magnitudes are presented. The consequences of the proposed rates are considered and their performance is tested numerically.

2. Experimental

The experiments were carried out in chamber A ($V = 200\,m^3$) of the two EUPHORE chambers available at CEAM in Valencia, Spain. The full details concerning the operation of the chamber and the associated instruments are discussed elsewhere (Becker, 1996), and only a brief description of the features particularly relevant to this work is given below. The FEP foil covered aluminium floor panels are water cooled to reduce solar heating of the chamber and maintain realistic atmospheric temperatures during the experimental runs. Clean air is supplied by a screw air compressor and purified by means of a filter system (Zander KEA, 1400) using pressure swing regeneration cycles with molecular sieve 4 Å to reduce water and carbon dioxide content, and an active charcoal filter bed to absorb VOC and NO_x components. NO_x components in the purified air are below 50 ppt, which is the detection limit of the ECO Physics NO_x analyser CLD ALppt770 with a PLC760 photolytic converter. CO and ozone were measured with Thermo Environment 48C and Monitor Labs 9810A monitors, respectively, averaged over 1 minute intervals.

In order to detect nitrous acid and formaldehyde with high accuracy, two newly installed, continuously operating monitors were used with detection limits of 3 ppt and 50 ppt (1σ), respectively. The accuracy of the HONO and HCHO monitors (LOPAP®, University of Wuppertal, Kleffmann *et al.* (2002) and Aero Laser AL4021, Germany, respectively) is based on liquid calibration standards and is better than 10%.

The 4π steradian actinic flux was determined by means of downward and an upward looking two filter radiometers (Schmitt, Glashütten) in the centre of the simulation chamber, 50 cm above the chamber floor, to determine the photolysis frequency j_{NO_2}, as measure of the photochemical activity.

The timelines of the investigated experiments are presented in the corresponding concentration graphs. The chamber was closed in the time intervals denoted by shaded areas. Vertical lines mark times when a compound was injected, or when the relative humidity was changed. In experiment I 200 ppm CO and 200 ppb HCHO was added. In experiment II 180 ppm CO and 5 ppb NO_2, while during experiment III 1000 ppm H_2 and 80 ppb HCHO was injected.

The determination of HONO and HCHO wall production rates were based on experiments I–III. The peak O_3 concentration was ~35 ppb, ~10 ppb and ~50 ppb in experiments I, II and III, respectively. In all three cases, HONO wall production was observed, and in experiments II and III, the HCHO concentration was also increased. The relative humidity (*RH*) was varied between 0% and 15%. The overall temperature range during the three experiments was from 287 K to 300 K.

3. The model

The Master Chemical Mechanism version 3.1 (MCMv3.1) is a comprehensive tropospheric chemical mechanism that describes the tropospheric oxidation of the main emitted volatile organic compounds (see Saunders *et al.*, 2003) and also website http://mcm.leeds.ac.uk/MCM/). In this work, the subset describing CH_4 oxidation, which includes HCHO chemistry, was used, supplemented with the inorganic reaction set of MCMv3.1. This mechanism contains 64 reactions of 23 species. The methane subset was chosen, because CH_4 produces detectable amounts of HCHO, as shown by preliminary model calculations. However, it should be noted that the HCHO production by methane is much lower than the HCHO production needed for the observed HCHO concentrations. The initial CH_4 concentration was always set to 1800 ppm, since it was not removed by the air

purification system. No auxiliary mechanism, i.e. reaction steps describing wall processes was included in the model.

Some of the rate parameters were updated from those given in MCMv3.1, based on the latest IUPAC recommendations (Atkinson *et al.*, 2004). In addition to the changes included by Zádor *et al.* (2005), the most significant updates were the rate coefficient of reaction $CH_3O_2 + NO_3$, which has changed by +41% to 1.3×10^{-12} cm^3 molecule^{-1} s^{-1}, while that of $OH + CH_4$ was increased by 3% at 298 K.

Photolysis rate coefficients of several species were updated using TUV4.2 (Tropospheric Ultraviolet & Visible Radiation Model version 4.2, Madronich and Flocke, 1998; Madronich, 2003). A significant difference between field and chamber experiments is the large albedo (∼0.5) of the latter, which was determined from the 2π j_{NO_2} measurements in upward and downward directions. Corrections were also made for the wavelength dependent transmission of the FEP Teflon film (74% at 290 nm, 80% at 350 nm and 90% above 450 nm). Apart from the albedo and the absorbance of the foil, standard atmospheric values were used in the radiation transfer model (e.g. standard US ozone column, standard temperature profile etc, according to the MCM protocol). The photolysis rates obtained from TUV4.2 as a function of solar zenith angle (θ) were used to determine the *l*, *m* and *n* parameters used in MCM according to the protocol of Saunders *et al.* (2003):

$$j(\theta) = l \cos^m(\theta) e^{-n \sec(\theta)} \tag{1}$$

The spectroscopic data were all taken from the latest IUPAC evaluation, except for the j_{NO_2} quantum yield (TUV4.2 values used), and j_{NO_3} (absorption cross section from Graham and Johnston (1978) for <600 nm and, DeMore *et al.* (1997) for >600 nm were used). The updated parameters are as follows: $j_{O_3}[7.726 \times 10^{-5}, 2.373, 0.165]$, $j_{NO_2}[1.927 \times 10^{-2}, 0.866, 0.136]$, $j_{HONO}[3.475 \times 10^{-3}, 0.908, 0.134]$, $j_{HCHO,molecular}[7.870 \times 10^{-5}, 1.359, 0.153]$, $j_{HCHO,radical}[8.337 \times 10^{-5}, 1.166, 0.125]$, $j_{H_2O_2}[1.409 \times 10^{-5}, 1.372, 0.098]$, $j_{NO_3 \rightarrow NO_2}[4.123 \times 10^{-2}, 0.516, 0.119]$, $j_{NO_3 \rightarrow NO_2}[3.258 \times 10^{-1}, 0.541, 0.129]$, $j_{HNO_3}[1.304 \times 10^{-6}, 1.844, 0.092]$, where the numbers in the brackets are the *l*, *m* and *n* parameters, respectively.

To investigate the effect of the update of the spectroscopic parameters on the photolysis rate coefficients, ratios $r_X = j_X/j_{NO_2}$ were calculated with both the original and the updated parameterisation, where *X* denotes a photolyte other than NO_2. This comparison is adequate, because during the simulations photolysis parameters are scaled to j_{NO_2} values, since only j_{NO_2} was measured. The analysis showed that the greatest differences between the new and the old parameterisation are in $r_{H_2O_2}$ (−15%), r_{HONO} (−19%), $r_{HCHO,molecular}$ (−22%), where the percentage values correspond to 30° solar zenith angle. It should be noted that the scaling of photolysis rate coefficients with j_{NO_2} automatically provides accurate modelling of the opening and closing of the chamber, which usually takes about 5 min.

Initial NO and NO_2 concentrations were assumed to be zero in experiment I, as the data at the beginning of the experiments scattered within the zero noise region. For experiments II and III, initial NO_2 was assumed to be equal to the average of the first few datapoints, which yielded 0.3 ppb in both cases. This might be a contamination effect from a previous experiment. Dilution rates were derived either from SF_6, or from CO concentration profiles. Injection of species Y was modelled by a reaction producing Y, with nonzero rate coefficient only during the period of injection which is not an instantaneous process, taking at least 5 min. The rate coefficient was tuned to produce the observed concentration rise, keeping all other parameters at their nominal values.

4. Estimation of the mean values of the HONO and HCHO wall production rates

HONO and HCHO measurements were available for all experiments. Since these species were certainly not of gas phase origin, their modelled concentrations were not calculated from the chemical kinetic differential equations, but were constrained to their measured values. Although the concentration of HCHO in the HCHO + CO (I) experiment could be primarily interpreted by chemical reactions and dilution, [HCHO] was still constrained to the measured values to preserve comparability with results from the other two experiments.

The aim was to determine the rates of the following proposed wall reactions:

$$\mathrm{HONO_{wall}} \rightarrow \mathrm{HONO} \tag{R1}$$

$$\mathrm{HCHO_{wall}} \rightarrow \mathrm{HCHO} \tag{R2}$$

The quantification of the production rate of both HONO and HCHO was based on the following general equation:

$$\frac{\mathrm{d[X]_{obs}}}{\mathrm{d}t} = W(\mathrm{X})_{\mathrm{EUPHORE}} + \\ + \sum_P k_P[\mathrm{A}_P][\mathrm{B}_P] + \sum_P j_P[\mathrm{A}_P] - [\mathrm{X}]_{\mathrm{obs}} \left(\sum_L k_L[\mathrm{A}_L] + \sum_L j_L + D \right), \tag{2}$$

where the left hand side is the gradient of the observed concentration $[\mathrm{X}]_{\mathrm{obs}}$, while the right hand side includes sources (positive terms) and sinks (negative terms). The first source term is the wall production in EUPHORE, $W(\mathrm{X})_{\mathrm{EUPHORE}}$. The next term is the chemical production by the core mechanism (P), where k_P, $[\mathrm{A}_P]$ and $[\mathrm{B}_P]$ are the appropriate rate coefficient and concentrations, respectively. It is followed by the contribution of photolysis of species A_P yielding species X with rate coefficient j_P. The loss (L) terms are similar, except for the first order dilution (D), which was $\sim 1 \times 10^{-5}\ \mathrm{s}^{-1}$. In the experiments, the dilution rate was determined by monitoring the concentration of a non-reactive trace compound (SF_6). From the above equation, it is possible to express the wall production rate as a function of time. The production and loss terms can easily be calculated from the model runs as a function of time. The data were smoothed prior to determination of the derivative of the observed concentration profile, to overcome the noise.

Based on MCMv3.1, the following equation was used in the case of HONO:

$$W(\mathrm{HONO})_{\mathrm{EUPHORE}} = \frac{\mathrm{d[HONO]_{obs}}}{\mathrm{d}t} - k_{\mathrm{OH+NO}}[\mathrm{OH}][\mathrm{NO}] + \\ + [\mathrm{HONO}]_{\mathrm{obs}}(k_{\mathrm{OH+HONO}}[\mathrm{OH}] + j_{\mathrm{HONO}} + D) \tag{3}$$

and the appropriate equation for HCHO is:

$$W(\mathrm{HCHO})_{\mathrm{EUPHORE}} = \frac{\mathrm{d[HCHO]_{obs}}}{\mathrm{d}t} - (k_{\mathrm{CH_3O_2}}[\mathrm{CH_3O_2}] + \\ + k_{\mathrm{CH_3OH+OH}}[\mathrm{CH_3OH}][\mathrm{OH}] + k_{\mathrm{OH+CH_3NO_3}}[\mathrm{OH}][\mathrm{CH_3NO_3}] + \\ + k_{\mathrm{CH_3O}}[\mathrm{CH_3O}] + k_{\mathrm{OH+CH_3OOH}}[\mathrm{OH}][\mathrm{CH_3OOH}]) + \\ + [\mathrm{HCHO}]_{\mathrm{obs}}(k_{\mathrm{OH+HCHO}}[\mathrm{OH}] + k_{\mathrm{NO_3+HCHO}}[\mathrm{NO_3}] + \\ + j_{\mathrm{HCHO,molecular}} + j_{\mathrm{HCHO,radical}} + D) \tag{4}$$

Rohrer *et al.* (2005) used a different approach. They fitted the parameters of an empirical rate expression describing HONO formation on the chamber wall, to the observed NO and NO_2 profiles; the parametric equation reproduced the HONO concentration profile with good accuracy. This approach was not feasible in the present analysis, since the NO_2 measurements were much more noisy than those of Rohrer *et al.* (2005). However, it should be noted that fixing HONO to the measured values reproduced the NO, NO_2 and O_3 profiles with good accuracy in the simulations of the experiments investigated. The main advantage of our method is that it does not presume a functional form for the wall production rate. The rate data obtained can be analysed to determine any dependencies on experimental parameters and also experiment-to-experiment variations are easier to observe.

5. Determination of the uncertainty range of the calculated concentrations and of the wall production rates

Uncertainty analysis is a family of mathematical–statistical methods, which enables the investigation of various aspects of model output uncertainty based on the uncertainty of the input parameters. Two types of uncertainty analysis, local and global were used for the investigation of our chamber experiments. These methods are complementary, providing different, but equally important information about the system (Saltelli *et al.*, 2000; Zádor *et al.*, 2005).

Uncertainty factors for the elementary reaction rate coefficients were collected from chemical kinetic databases (Atkinson *et al.*, 2004; Sander *et al.*, 2002), which are critically evaluated and frequently updated. These factors were converted to the variance of the parameters using the method described in the articles of Turányi *et al.* (2002) and Zádor *et al.* (2005). The probability density functions (*pdf*s) of the parameters were also established; lognormal distributions were assumed for the rate coefficients, and normal distributions for the initial and constrained concentrations. The uncertainty of the rate of injection during the experiments was taken as 0.05–0.1 depending on the species and assuming lognormal distribution. HONO and HCHO concentrations were assumed to be normally distributed parameters with the uncertainty of the measurement. Uncertainty of the initial CH_4 concentration was ± 50 ppm, that of CO was ± 100 ppm if not measured and $\pm 5\%$ if measured, for both cases assuming normal distribution. All distributions were truncated at 2σ and in addition a zero cut-off was used in the case of normal distribution, eliminating negative values.

5.1. Local uncertainty analysis

Local uncertainties were calculated by combining first-order local sensitivity coefficients, $\partial c_i/\partial p_j$ (Turányi, 1990) with uncertainty estimates of the input parameters $\sigma^2(p_j)$ in the same way as it was discussed in the papers of Turányi *et al.* (2002) and Zádor *et al.* (2005).

In the cases of the present simulations we were interested in the integrated effect of parameter uncertainties, rather than their effect at a given timepoint of the experiment. Therefore, sensitivities were calculated numerically by taking the integrated difference of the nominal

concentration profiles and the perturbed ones for the whole experiment:

$$\sigma_j^2(I(c_i)) = \sigma^2(p_j)\left(\frac{\sum_{q=1}^{N}\left(c_{i,q} - c_{i,q}^0\right)}{N \times \Delta p_j}\right)^2 \quad (5)$$

where $\sigma_j^2(I(c_i))$ is the contribution of parameter p_j to the uncertainty of concentration c_i during the whole experiment, Δp_j is the perturbation of parameter p_j, which was $0.01p_j$ in the calculations, and N is the number of discrete timepoints where the concentrations were evaluated (typically 30 points per hour simulated). In the case of rate coefficients, Equation (5) holds if p_j is replaced by $\ln k_j$.

5.2. Monte Carlo simulations with Latin hypercube sampling

To provide the exact and unbiased *pdf* of the output values (Saltelli *et al.*, 2005), Monte Carlo (MC) type simulations were also carried out. To keep the number of runs as low as possible, Latin hypercube sampling (Helton and Davis, 2002; Saltelli *et al.*, 2000) was applied, which covers the parameter space with minimal sample size in an unbiased manner. The number of runs was 1000 for each of the experiments.

In this work, MC simulations were used not only to estimate the uncertainties in the calculated concentrations, but also, to approximate the uncertainty in the HONO and HCHO net production rates, d[X]/dt. This was done by evaluating Equations (3) and (4) in all MC runs, parallel to the calculation of the concentration profiles. This provided the 1σ standard deviation of the net production rate calculated by the model.

6. Results

6.1. The HCHO + CO experiment (I)

Experimental and model concentrations are shown in Figure 1. Agreement of the modelled and the measured values was excellent for ozone and the calculated NO_2 concentrations were also in good agreement with the measurements.

Results of the local uncertainty analysis (see Figure 2a) show that uncertainties in the HONO photolysis rate coefficient and the measured [HONO] make the greatest contributions to the uncertainties in the calculated ozone, NO_2 and OH concentrations, while uncertainties in the rate of HCHO photolysis to form radicals and the self-reaction rate coefficient also contribute the uncertainty in [HO_2]. According to the Monte Carlo runs (see Table 1), [OH] is subject to the greatest uncertainty.

$W(\text{HONO})_{\text{EUPHORE}}$ was calculated according to Equation (3). Figure 1e shows that $W(\text{HONO})_{\text{EUPHORE}}$ was zero in the closed chamber; in the open chamber it was $(0.8-1.4) \times 10^{-4}$ ppb s^{-1} when the relative humidity was nearly zero, and increased to $(2.4-5.2) \times 10^{-4}$ ppb s^{-1}, when the relative humidity was increased to 7%. This observation suggests that HONO production is photoinduced and humidity enhanced. According to the MC simulations, the 1σ uncertainty of $W(\text{HONO})_{\text{EUPHORE}}$ was 2.4×10^{-5} ppb s^{-1} ($\sim$23%) for low production rates (RH zero) and was 8.3×10^{-5} ppb s^{-1} ($\sim$20%) when HONO production was greater (RH 7%). Note that for all experiments the rapid temporal changes in calculated HONO and HCHO production rates (see e.g. Figure 1e between 13:00 and 14:00) were due to changes in the actinic flux, caused by clouds.

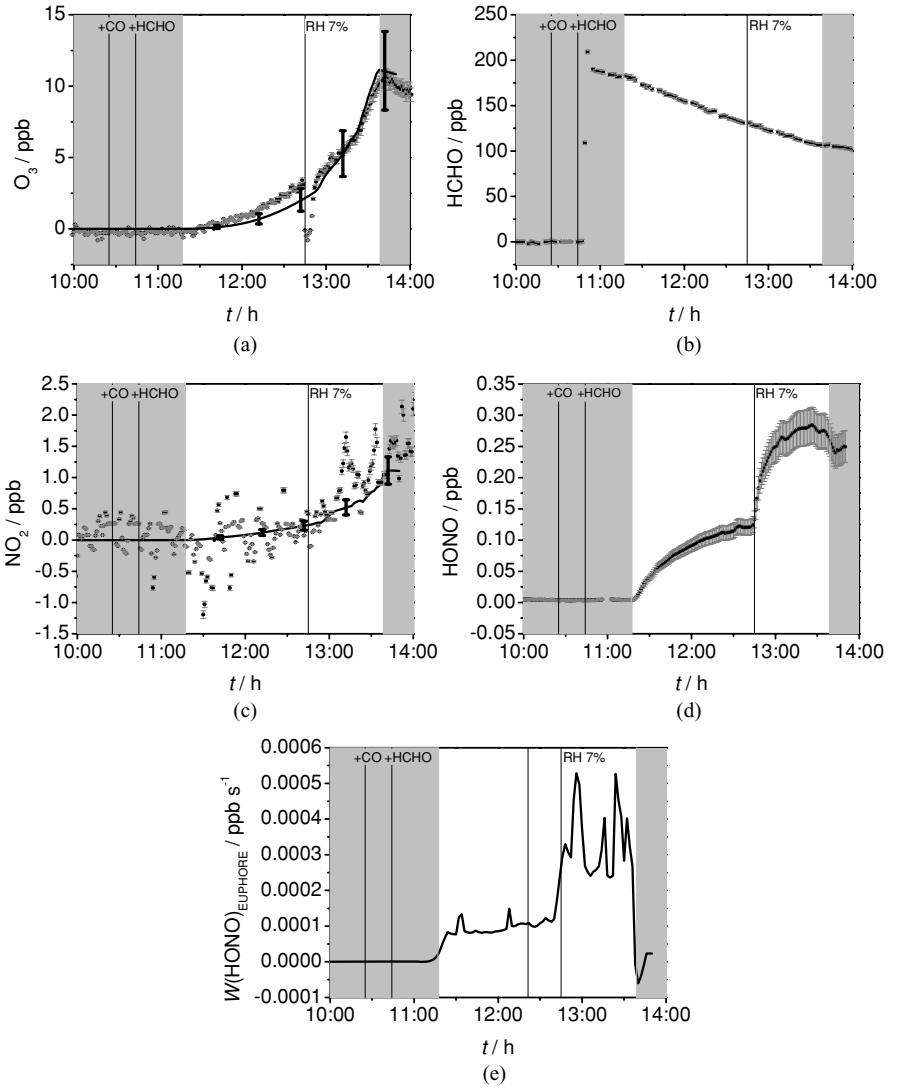

Fig. 1 The HCHO+CO experiment (I). (a) ozone, (b) formaldehyde (c) nitrogen dioxide (d) nitrous acid concentration profiles. Solid lines are the calculated values, while symbols are the measured ones with the experimental uncertainties represented as grey error bars. Thick black error bars are the 1σ uncertainties of the calculated values based on MC simulations. (e) Calculated HONO production rate

6.2. The CO experiment (II)

Results at the nominal parameter values are shown in Figure 3. In the first period, $[O_3]$ is accurately predicted, but at the end of the experiment, it is slightly overpredicted (12%). $[NO_2]$ is also predicted well by the model.

Local uncertainty analysis indicates (see Figure 2b) that the greatest uncertainty for each monitored species concentration was caused by the uncertainty of the constrained HONO concentration. Concentrations of O_3 and NO_2 are also uncertain due to the uncertainty in the

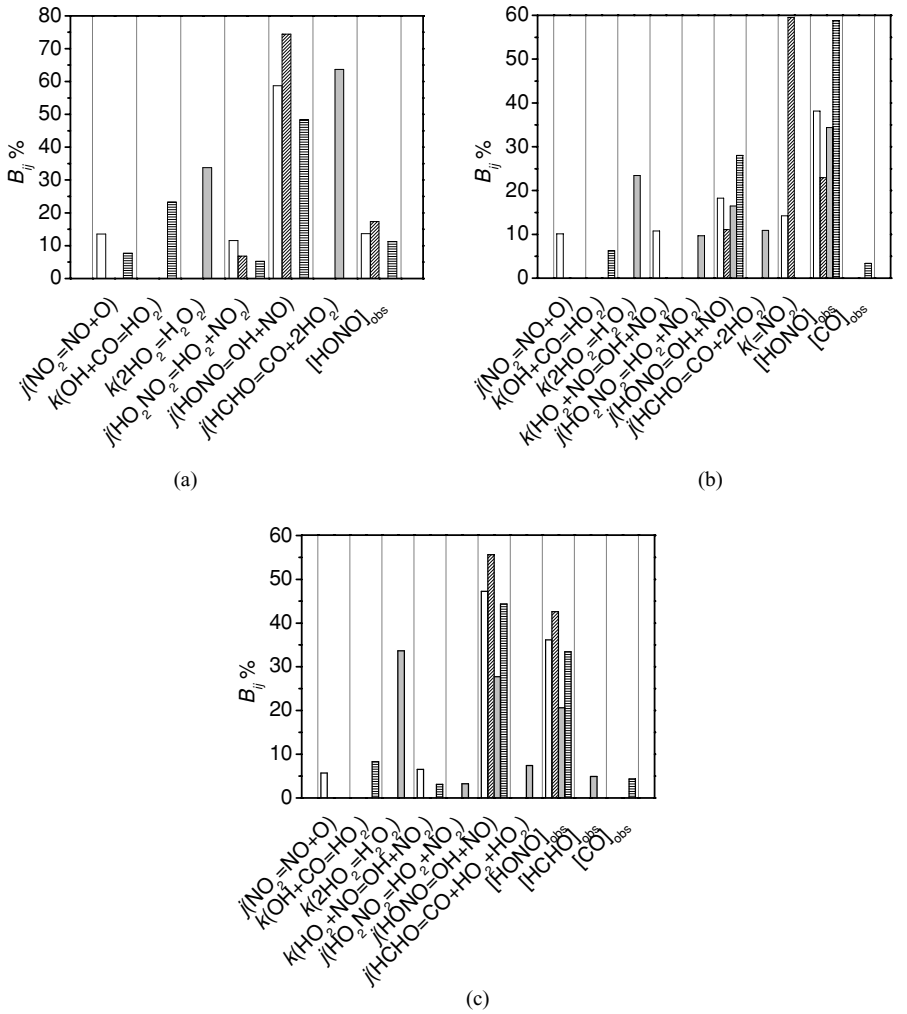

Fig. 2 Percentage contribution (B_{ij} %) of the indicated parameters to the uncertainty of the calculated concentration of O_3, NO_2, HO_2 and OH. (a) HCHO+CO experiment (I), (b) CO experiment (II), (c) H_2 experiment (III)

inlet quantity of NO_2. Uncertainty in the HONO photolysis rate plays an important role as well. The MC calculations show (see Table 1) that the 1σ standard deviation for all monitored species is around 10% at the time of the peak ozone concentration.

In the first part of the experiment, HONO production (see Figure 3e) was in the range $(0.7–1.5) \times 10^{-4}$ ppb s^{-1}, and after the injection of NO_2 it was $(1.2–2.6) \times 10^{-4}$ ppb s^{-1}. The 1σ uncertainty of the HONO production rate, according to the MC simulations, is 2.7×10^{-5} ppb s^{-1} in the first period of the experiment. No HONO production was observed in the dark.

The HCHO production rate as calculated by Equation (4), is presented in Figure 3f; it is approximately constant and is in the range of $(3.5–6.1) \times 10^{-4}$ ppb s^{-1}. There was no HCHO formation while the chamber was closed.

Table 1 Results of the MC analysis. The mean and the 1σ uncertainties are presented, the latter is also expressed as percentage. Concentrations are in ppb, and belong to the time of the peak ozone concentration

	Mean	1σ	%
HCHO + CO experiment (I)			
O_3	10.9	2.04	19
NO_2	1.12	0.18	17
$HO_2 \times 10^{-2}$	18.2	3.89	21
$OH \times 10^{-6}$	1.66	0.562	34
CO experiment (II)			
O_3	25.6	3.02	12
NO_2	3.75	0.380	10
$HO_2 \times 10^{-2}$	3.59	0.348	10
$OH \times 10^{-6}$	4.72	0.576	12
H_2 experiment (III)			
O_3	60.0	11.0	18
NO_2	3.02	0.610	20
$HO_2 \times 10^{-2}$	6.11	0.465	8
$OH \times 10^{-5}$	6.92	1.22	18

6.3. The H_2 experiment (III)

Modelled and measured concentration profiles for the H_2 experiment are shown in Figure 4. Ozone and NO_2 concentrations are clearly overpredicted at the end of the experiment (both by 40%).

According to the local uncertainty analysis (see Figure 2c), the uncertainties in the HONO concentration uncertainty and in the HONO photolysis rate caused most of the uncertainty in the calculated values of all four monitored variables. The uncertainty in its self-reaction rate coefficient also contributes to the uncertainty in the calculated HO_2 concentration. Global uncertainty estimates are low for HO_2 (8%), and around 20% for the other species (see Table 1).

The HONO wall production rate was $(1.7–3.0) \times 10^{-4}$ ppb s^{-1} under low humidity conditions, and increased to $(3.8–5.5) \times 10^{-4}$ ppb s^{-1}, when the humidity was higher (see Figure 4e). Zero HONO production was calculated in the absence of solar radiation. The calculated 1σ uncertainty is 5.8×10^{-5} ppb s^{-1} for 0% *RH*, and increased to 8.8×10^{-5} ppb s^{-1}, when humidity was increased. Estimation of HCHO production yielded $(2.7–7.4) \times 10^{-4}$ ppb s^{-1}, and again, no dark wall HCHO production was observed (see Figure 4f).

7. Discussion

7.1. General conclusions from uncertainty analysis

Since complete agreement between modelled and observed concentration profiles is not expected, it is meaningful to ask, whether the observed discrepancies are statistically significant or not. Comparing the measured and calculated concentration profiles in Figures 1, 3 and 4 with the results of the MC simulations (see the error bars in the figures and also Table 1), the following conclusions can be drawn:

1. In the HCHO + CO experiment (I, see Figure 1), excellent agreement was found between the measured and the calculated concentrations of ozone and NO_2. In the CO experiment

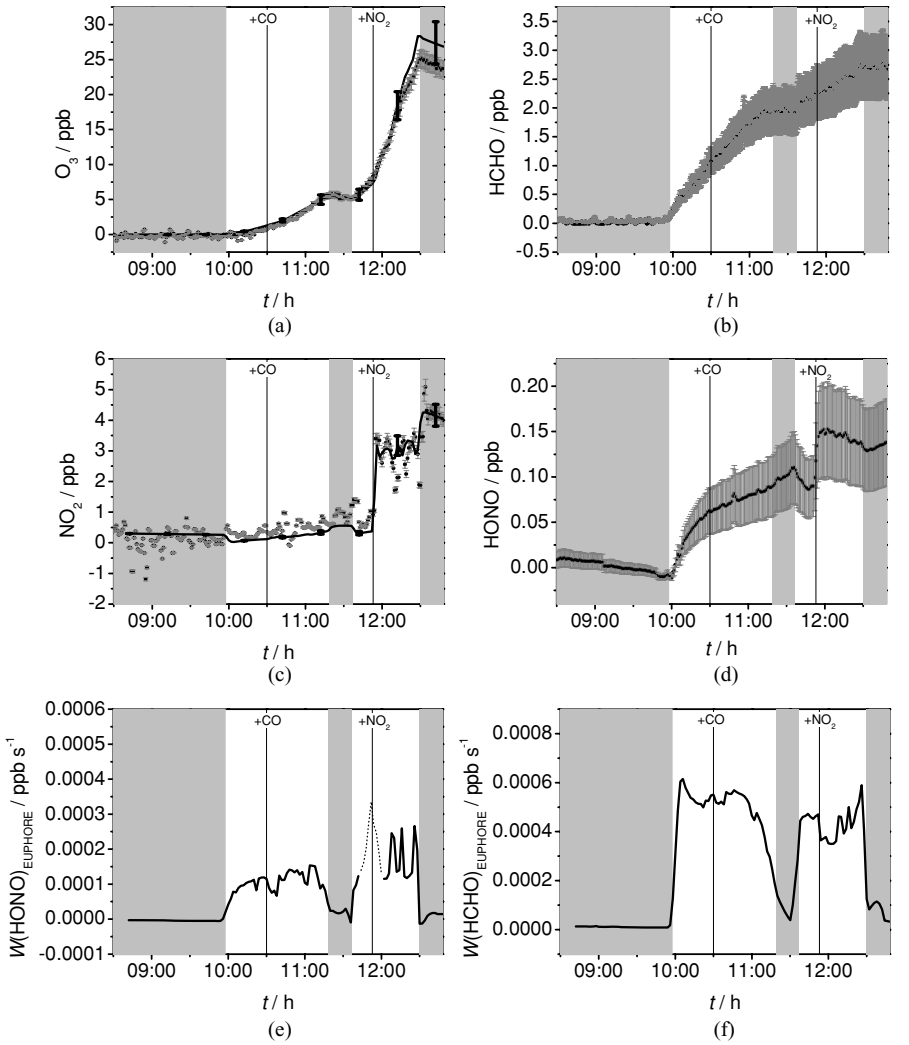

Fig. 3 The CO experiment (II). (a) ozone, (b) formaldehyde (c) nitrogen dioxide (d) nitrous acid concentration profiles. Solid lines are the calculated values, while symbols are the measured ones with the experimental uncertainties represented as grey error bars. Thick black error bars are the 1σ uncertainties of the calculated values based on MC simulations. (e) Calculated HONO and (f) HCHO production rates. Dotted line on (f) belongs to the time interval of NO_2 addition

(II, see Figure 3), the observed overprediction of ozone is not statistically significant, since the calculated and measured 1σ uncertainties overlap. In the H_2 experiment (III, see Figure 4), despite the good agreement for ozone and NO_2 at the beginning, overprediction is observed at the ozone peak, where the measurement and calculation overlap only at the 2σ level.

2. According to the local uncertainty analysis, the uncertainties for the measured [HONO] and the calculated j_{HONO} make the major contributions to the uncertainty in modelled [OH]. The accuracy of the [HONO] measurement is close to the current technological edge and

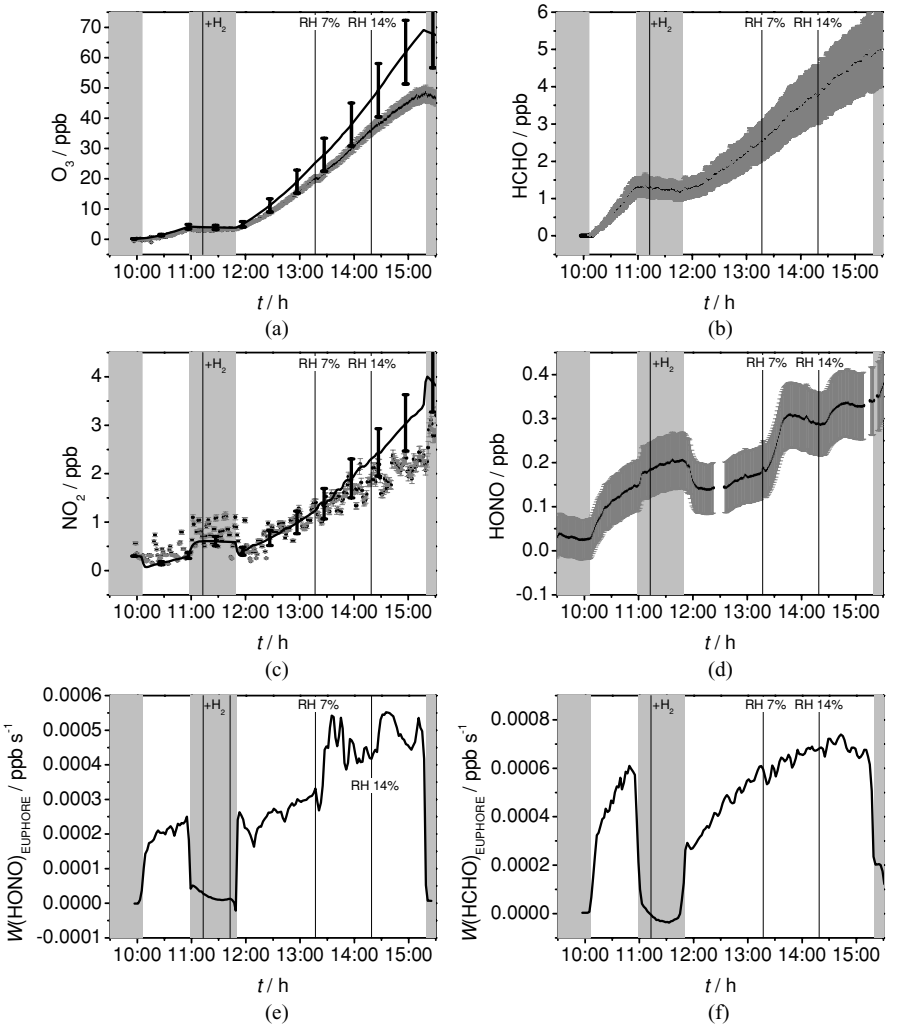

Fig. 4 The H_2 experiment (III). (a) ozone, (b) formaldehyde (c) nitrogen dioxide (d) nitrous acid concentration profiles. Solid lines are the calculated values, while symbols are the measured ones with the experimental uncertainties represented as grey error bars. Thick black error bars are the 1σ uncertainties of the calculated values based on MC simulations. (e) Calculated HONO and (f) HCHO production rates

its improvement is not expected in the near future. However, the uncertainty of the calculated [OH] could be significantly decreased by using a spectral radiometer in the chamber, and calculating j_{HONO} directly from the measured actinic flux data. Since the ozone concentration is closely linked to the OH concentration, it is not surprising that its uncertainty is linked to the same factors. In these zero-NO_x experiments, it is also evident that the major uncertainty factors in the calculated NO_2 concentration are also the same, since the wall production of HONO is the only NO_x source. The zero-NO_x experiments analysed in this work differ substantially from high NO_x smog chamber experiments, where the uncertainty contributions have been analysed and where the $\mathrm{OH} + \mathrm{NO_2} + \mathrm{M} \rightarrow \mathrm{HNO_3} + \mathrm{M}$

reaction was found to be the major source of uncertainty, as shown by Zádor *et al.* (2005). These HONO factors also make a contribution to the uncertainty in HO_2, but there are other significant uncertain factors, primarily the self-reaction and the HCHO photolysis.

The uncertainty analysis demonstrates that the concentrations of the key species have a high sensitivity to the reactions of HONO, and to a lesser extent to the reactions of HCHO, and hence indirectly to the wall production rate of HONO and HCHO. This means that the wall production rate of HONO and HCHO can be determined from the measured concentration profiles.

7.2. Characterisation of the wall production processes

It is desirable to quantify the production of HONO and HCHO in a parameterised manner, even if the determined expression is an empirical one. The resulting expressions can be used in models to account for chamber dependent radical sources. It is clear from Figures 1, 3 and 4 that the wall production of HONO and HCHO are both light driven; in addition, HONO production is enhanced by humidity. The temperature dependence of the processes is not apparent from these figures however, and it will be analysed in this section.

In the case of HONO wall production, a thorough analysis has shown that the data can be divided into two sets. The first set of points belongs to dry conditions (relative humidity below 2%), while the rest of the points belong to the more humid conditions (2–15%). The dry dataset was found to be dependent on j_{NO_2} and temperature; their ranges were 0–0.01 s^{-1} and 287–300 K, respectively. There is no high correlation (0.6) between temperature and light intensity. The following equation was used for the fitting:

$$W(\mathrm{HONO})^{\mathrm{dry}}_{\mathrm{EUPHORE}} = a \times j_{NO_2} \times \exp(-T_0/T) \tag{6}$$

where a and T_0 are fitted parameters. The fit resulted in $a = 7.3 \times 10^{21}\,\mathrm{cm}^{-3}$, and $T_0 = 8945$ K. Figure 5a shows a plot of $W(\mathrm{HONO})^{\mathrm{dry}}_{\mathrm{EUPHORE}}/(a \times \exp(-T_0/T))$ vs. j_{NO_2} graph to demonstrate the first order dependence of the HONO wall production rate on j_{NO_2}. While there is considerable scatter in the graph, the correlation coefficient is 0.88. The three distinguishable groups of points in Figure 5a belong to the three experiments; this shows the magnitude of the experiment-to-experiment variability. Considering however that the underlying processes are slow, the observed amount of scatter is acceptable. Figure 5b shows $\ln(W(\mathrm{HONO})^{\mathrm{dry}}_{\mathrm{EUPHORE}}/j_{NO_2})$ vs. $1/T$. Again, the three experiments differ considerably, but the $\exp(-T_0/T)$ dependence is clearly visible.

For the datapoints at a relative humidity of 2–15%, temperature dependence was not detectable. In this case we found that humidity acts as an enhancement factor on the top of the HONO production determined for the dry case (the correlation between relative humidity and j_{NO_2} was zero). Therefore, the applied expression applied was:

$$W(\mathrm{HONO})^{\mathrm{humid}}_{\mathrm{EUPHORE}} = W(\mathrm{HONO})^{\mathrm{dry}}_{\mathrm{EUPHORE}} + j_{NO_2} \times b \times RH^q \tag{7}$$

$W(\mathrm{HONO})^{\mathrm{dry}}_{\mathrm{EUPHORE}}$ was $5.5 \times 10^8\,\mathrm{cm}^{-3} \times j_{NO_2}$, calculated with the average temperature of these datapoints (296 K, the temperature range was 290–300 K). The fit gave $b = 5.8 \times 10^8\,\mathrm{cm}^{-3}$ and $q = 0.36$ (RH is in percentages). The performance of the fit is demonstrated in Figure 5c in a similar manner as in the dry case, by plotting $W(\mathrm{HONO})^{\mathrm{humid}}_{\mathrm{EUPHORE}}/(5.5 \times 10^8 + b \times RH^q)$ vs. j_{NO_2}. The points are aligned along a line, and the correlation is excellent (0.97). It should be added that the humidity was increased in steps. For the fits, points belonging

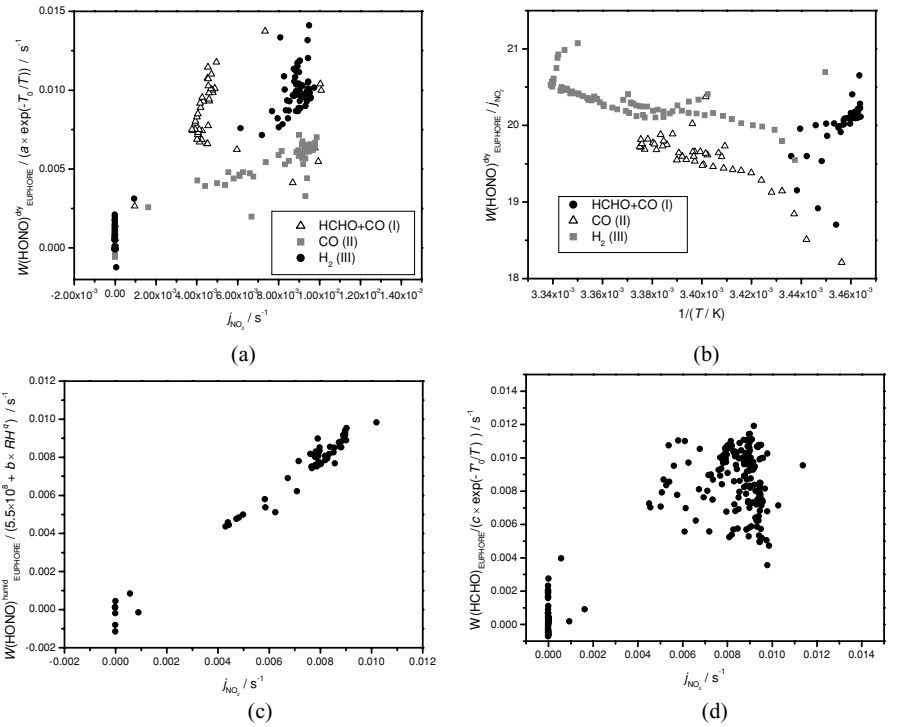

Fig. 5 Demonstration of the fits of (a, b) Equation (6) for HONO wall production in the case of low humidity (<2%), (c) Equation (7) for HONO wall production in the case of higher humidity (2–15%), (d) Equation (12) for HCHO wall production

to the plateaus were utilised only. During the increase of humidity we found a transient behaviour, which is most probably arises from the finite time for the relative humidity to adjust; a sprayer was used to add water into the chamber.

Rohrer *et al.* (2005) found that NO_2 does not influence the rate of wall HONO production. In our case it seems that the addition of NO_2 in experiment II has slightly enhanced HONO production; the value of parameter a is 8.8×10^{21}, when using the same T_0 value. Although the current experiments did not contain enough information for a quantitative description of the wall HONO production as a function of NO_2 concentration, it is possible to carry out a simple calculation. For $j_{NO_2} = 10^{-3}\ s^{-1}$, under dry conditions the HONO production rate in the absence of added NO_2 is 6.7×10^6 molecule $cm^{-3}\ s^{-1}$ using Equation (7), while with 5 ppb added NO_2 it is 8.4×10^6 molecule $cm^{-3}\ s^{-1}$; a difference of 1.4×10^6 molecule $cm^{-3}\ s^{-1}$. Using the current parameterisation in MCMv3.1 for the assumed $NO_2 \rightarrow$ HONO heterogeneous reaction ($k = 0.7 \times 10^5\ s^{-1}$) 1.2×10^6 molecule $cm^{-3}\ s^{-1}$ HONO production rate is obtained originating from the added 5 ppb NO_2, which means that if the observed enhancement due to NO_2 is correct, the two numbers are in a very good agreement. The influence of added NO_2 should be further investigated experimentally, since the apparent HONO production can also be affected by contamination effects.

It is also interesting to compare our numerical results to those of Rohrer *et al.* (2005). They used a different empirical equation for the characterisation of the HONO wall production. At 300 K, $j_{NO_2} = 8 \times 10^{-3}\ s^{-1}$ (typical for the experiments carried out in EUPHORE)

and $RH = 0\%$ the rate of HONO formation in the SAPHIR chamber is $7.2 \times 10^5\,\mathrm{cm^{-3}\,s^{-1}}$ (using one of their two parameter sets), while in EUPHORE it is $5.4 \times 10^6\,\mathrm{cm^{-3}\,s^{-1}}$. Increasing *RH* to 15%, gives rates of $1.9 \times 10^6\,\mathrm{cm^{-3}\,s^{-1}}$ and $1.7 \times 10^7\,\mathrm{cm^{-3}\,s^{-1}}$ for SAPHIR and EUPHORE, respectively. That is the HONO production rate in the EUPHORE chamber is about one order of magnitude higher than in SAPHIR. The surface-to-volume ratios of both chambers are $\sim 1\,\mathrm{m^{-1}}$, and also the volumes are comparable ($V_{\mathrm{SAPHIR}} = 270\,\mathrm{m^3}$ and $V_{\mathrm{EUPHORE}} = 200\,\mathrm{m^3}$), so this cannot be the cause of the observed differences. A possible reason might be that experiments in SAPHIR are usually carried out using lower concentrations.

It is possible to estimate the number of HNO_3 monolayers on the surface of the FEP Teflon as a function of relative humidity. Surface *A* of the $200\,\mathrm{m^3}$ hemispherical chamber is around $200\,\mathrm{m^2}$, and this surface is entirely made of Teflon, except for the negligible surface area of the instruments. In the mechanism of Zhou *et al.* (2002), the rate determining step for the wall HONO formation is the photolysis of adsorbed HNO_3 on the walls. Assuming a steady-state for HNO_3 on the wall, and that the photolysis rate on the wall is the same as in the gas phase, the amount of HNO_3 per unit area ($\rho_{\mathrm{HNO_3}}$) is given by:

$$\rho_{\mathrm{HNO_3}} = \frac{V \times W(\mathrm{HONO})^{\mathrm{humid}}_{\mathrm{EUPHORE}}}{N_A \times j_{\mathrm{HNO_3}} \times A} = \frac{V \times j_{\mathrm{NO_2}} \times (5.5 \times 10^8 + b \times RH^q)}{N_A \times j_{\mathrm{HNO_3}} \times A}, \tag{8}$$

where N_A is the Avogadro number. The $j_{\mathrm{HNO_3}}/\mathrm{NO_2}$ ratio was calculated by TUV4.2 taking the effect of the foil into account. At 30° solar zenith angle:

$$j_{\mathrm{HNO_3}} \approx j_{\mathrm{NO_2}}/15500 \tag{9}$$

At $T = 298\,\mathrm{K}$, this density corresponds to 2–3 layers of HNO_3 at 5% *RH*, increasing to 6–7 layers at 15% *RH*, if the molecular area is calculated from the bulk HNO_3 density ($d = 1.4\,\mathrm{g\,mol^{-1}}$). These numbers seem to be somewhat high, which questions the applicability of the mechanism proposed by Zhou *et al.* (2002) for FEP Teflon surfaces. However, it should be noted that the calculation above assumed a perfectly smooth surface and a photolysis rate identical to that in the gas-phase. Although this latter assumption may be valid, the first one is definitely not true, since Teflon is a highly porous material (Rye and Martinez, 1989) and the actual surface area is likely to be significantly larger than the geometrical value. Thus the mechanism of Zhou *et al.* (2002) cannot be excluded on this basis.

As described in the paper of Rohrer *et al.* (2005), it is useful to compare the OH production from HONO photolysis $P(\mathrm{OH})_{\mathrm{HONO}}$ and from ozone photolysis $P(\mathrm{OH})_{\mathrm{O_3}}$. The photostationary HONO concentrations in EUPHORE are 0.13 ppb and 0.28 ppb at 0% and 15% *RH*, respectively (298 K). Our calculation was identical to that of Rohrer *et al.* (2005) except that we used

$$j_{\mathrm{HONO}} = j_{\mathrm{NO_2}}/4.6 \tag{10}$$

and

$$j_{\mathrm{O^1D}} = j_{\mathrm{NO_2}}/302 \tag{11}$$

obtained from TUV4.2 for solar zenith angle 30° ($j_{\mathrm{NO_2}} = 8 \times 10^{-3}\,\mathrm{s^{-1}}$) taking the absorbance of the Teflon foil into account, while Rohrer *et al.* (2005) used scaling factors of 5.8 and 333 in the denominators of Equations (10) and (11), respectively. The differences

can be attributed to that they used of literature values, while we used calculated data, taking the albedo and the absorption of the chamber also into account. Our results show that in the investigated 0–15% relative humidity range, the production of OH from HONO is about a factor of 2 higher than the OH production from 100 ppb ozone. This result emphasises the importance of accurate quantitative characterisation of HONO production.

HCHO formation on the chamber wall (R2) did not show any correlation with humidity. It was found that it is highly dependent on j_{NO_2}, and also temperature influences the process. Therefore, the following function was fitted to the data of experiments II and III:

$$W(\mathrm{HCHO})_{\mathrm{EUPHORE}} = c \times j_{NO_2} \exp(-T_0'/T) \tag{12}$$

Calculations yielded $c = 3.1 \times 10^{17}\,\mathrm{cm}^{-3}$ and $T_0' = 5686\,\mathrm{K}$. The first order dependence of HCHO wall production on j_{NO_2} is shown in Figure 5d. Again, the scatter is significant, but considering the slow rate of the process, it is acceptable. Also, since the absorption bands of HCHO are further from those of NO_2 than those of HONO, therefore the calculated values of j_{HCHO} from the j_{NO_2} measurements has a higher uncertainty, good correlation is not expected.

Considering the wall production as the main formaldehyde source at the conditions of experiments II and III, (justified by model calculations) and the photolysis loss terms for HCHO:

$$\mathrm{HCHO} + h\nu \rightarrow 2\mathrm{HO}_2 + \mathrm{CO} \tag{R3}$$

$$\mathrm{HCHO} + h\nu \rightarrow \mathrm{H}_2 + \mathrm{CO} \tag{R4}$$

and using TUV4.2 values of

$$j_{\mathrm{HCHO,radical}} = j_{NO_2}/324 \tag{13}$$

$$j_{\mathrm{HCHO,molecular}} = j_{NO_2}/210 \tag{14}$$

it is possible to calculate the photostationary HCHO concentration, which yields 8.2 ppb at 298 K, and solar zenith angle 30° ($j_{NO_2} = 8 \times 10^{-3}\,\mathrm{s}^{-1}$). Calculating the HO_2 production from HCHO photolysis at its steady state gas-phase concentration using equation

$$P(\mathrm{HO}_2)_{\mathrm{HCHO}} = [\mathrm{HCHO}]_{\mathrm{ss}} \times 2 j_{\mathrm{HCHO,radical}} \tag{15}$$

gives $P(HO_2)_{HCHO} = 1.0 \times 10^7\,\mathrm{cm}^{-3}\,\mathrm{s}^{-1}$. This production is low, so it will not significantly affect the radical budget in low concentration experiments, unlike the OH production from HONO. On the other hand, HCHO wall production should be taken into account to obtain reliable formaldehyde concentrations when simulating experiments involving HCHO formed in gas-phase chemical reactions or added in low concentration to the chamber. Rohrer *et al.* (2005) observed HCHO wall production rates of $0–5.6 \times 10^{-5}\,\mathrm{s}^{-1}$ (0–0.2 ppb h^{-1}) in the SAPHIR smog chamber, which are also at least one magnitude lower than the ones in the EUPHORE chamber. The chemical mechanism of HCHO wall production in Teflon chambers is even less understood than that of HONO wall production, therefore we do not speculate on the mechanistic origin of the obtained expression.

As for the consequences for the future VOC–NO_x experiments to be carried out in EUPHORE, it is likely that in most cases the initial [HONO] derives from contamination of the injected NO_x, since in all the three investigated experiments, the initial HONO concentration

was found to be zero. Therefore, the initial HONO concentration is most probably proportional to the initial NO_x concentration. Although there is substantial variance in the magnitude of the continuous HONO wall source in the chamber, it is in the range of 5×10^{-3} ppb s^{-1}. A possible protocol to carry out very low NO_x concentration smog chamber experiments in EUPHORE is to open the chamber before the injection of the VOC/NO_x mixture, measure HONO and HCHO levels for about one hour, and then carry out the experiment as usual. This way, data obtained from the first hour can be used to estimate the actual background reactivity as shown in this paper.

7.3. Test cases for the obtained parameterisation

In order to check the validity and reliability of the parameters obtained, two further measurements of similar type were used. These experiments were carried out before the installation of the HONO and HCHO monitors, but concentration measurements of O_3 and NO_2 were available. In experiment IV 100 ppb HCHO, while in experiment V 50 ppb, 90 ppb and 110 ppb O_3 was added to the chamber.

In Figure 6, ozone and NO_2 concentrations are presented for the above experiments, with, and without the inclusion of wall reactions R1 and R2. For the calculation of the HONO

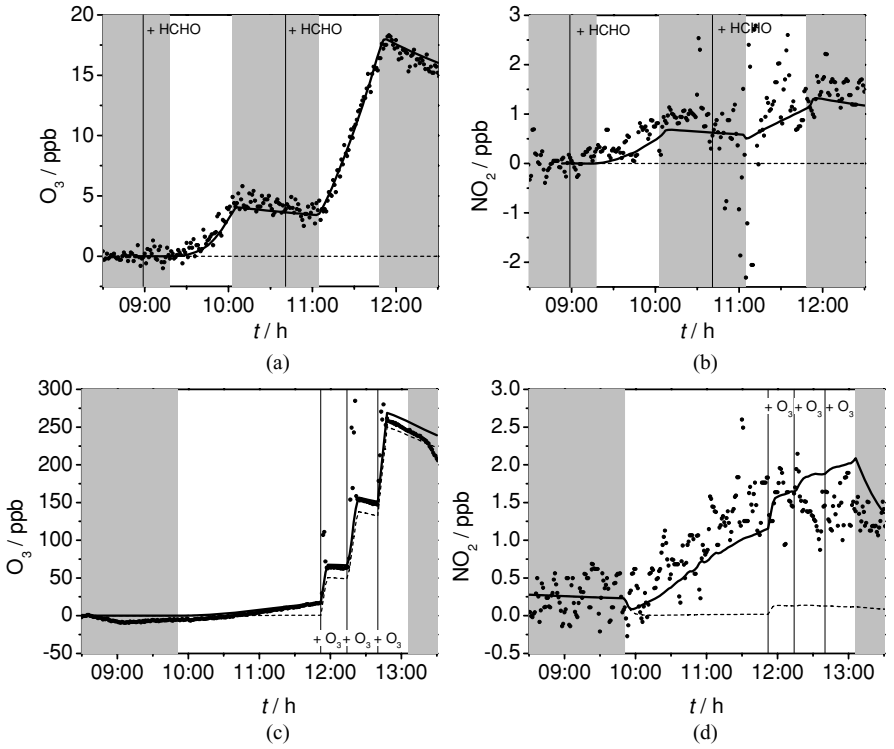

Fig. 6 Measured (symbols) and calculated (scattered line: without wall reactions R1 and R2, solid line: considering wall reactions R1 and R2) concentrations for (a) experiment IV, O_3, (b) experiment IV, NO_2, (c) experiment V, O_3, (d) experiment V, NO_2. Errors bars of the measurements are not shown for the sake of clarity, but are of the same magnitude as seen in Figures 1, 3 and 4

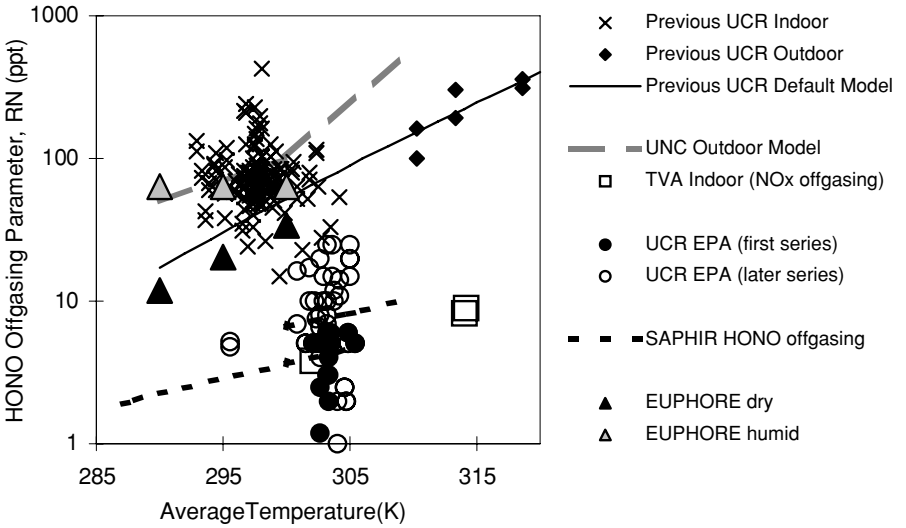

Fig. 7 HONO offgasing parameter (*RN*) in EUPHORE and in various other chambers. The original figure is a courtesy of J. P. W. Carter and the detailed comparison of the other values can be found in Carter *et al.* (2005).

wall production rate Equation (6) was used for experiment IV, as it is a dry experiment, and Equation (7) for experiment V, as it is a more humid experiment. For both cases, Equation (12) was applied for the simulation of HCHO production. It can clearly be seen that these reactions are essential for the modelling of the observed concentration profiles, and also that the parameterisation obtained from experiments I-III accounts for most of the reactivity observed.

8. Conclusions

Background radical sources in large environmental chambers are for a long time investigated phenomena. Our approach in this work was to simulate EUPHORE smog chamber measurements under very low NO_x conditions, where HONO and HCHO concentrations were measured by high sensitivity instruments. The concentrations of these two species were constrained to the measured values in the simulations and the wall production rates were determined from the model runs using the methane and inorganic subset of the Master Chemical Mechanism v3.1 with some updates, mostly for the photolysis parameters.

Most of the variability in O_2 and NO_2 concentrations could be interpreted by the presence of these two species, which means that from the many possible wall reactions, wall production of HONO and HCHO account for most of radical production not present in the gas-phase kinetic model. Local uncertainty analysis had shown that the main uncertainties of the calculated concentrations of ozone, NO_2, HO_2 and OH were caused by the uncertainties in the photolysis rate of HONO and the constrained HONO concentration. According to the Monte Carlo simulations, most of the discrepancies between the observed and the calculated concentration profiles are statistical, i.e. there is no evidence for systematic errors deriving from an inappropriate mechanism.

Wall production rates for HONO and HCHO were calculated for the experimental cases, and empirical formulae were used to express the j_{NO_2}, relative humidity and temperature dependence of their wall production rates. From our datasets it was possible to detect j_{NO_2} and temperature dependence of HONO wall formation in the case of dry conditions ($RH < 2\%$), while in the more humid region ($2\% < RH < 15\%$) the relative humidity dependence dominated. We also determined the effect of added NO_2 to the HONO formation rate and found that it is in good agreement with the current parameterization of MCMv3.1. For HCHO wall production only temperature and j_{NO_2} dependence was detected.

Comparing our results to those of Rohrer *et al.* (2005), we found that wall production rates in EUPHORE are one magnitude higher than in the SAPHIR smog chamber. We also present the magnitude of the HONO radical source in the EUPHORE chamber in a modified version of Figure 4 of Carter *et al.* (2005) in our Figure 7. It can be seen that the HONO offgassing measured in the EUPHORE chambers are in the low range of earlier UCR and UNC chambers, but are higher than the sources in TVA and new UCR chambers, as well as in the SAPHIR chamber. It was shown that the background HONO source produces about a factor of two more OH radicals than ozone at typical chamber concentrations (100 ppb) and HCHO wall production might be significant in low reactivity experiments.

Acknowledgements The authors would like to acknowledge the help of Dr. W. Bloss, and thank Prof. W. P. L. Carter for letting us use his figure. The work was supported by OTKA (grant number T043770) and instrumental grant (M042110) and this work was also part of the European Union project IALSI (contract No. EVR1-CT-2001-40013). Fundación CEAM is supported by the Generalitat Valenciana and Bancaixa. Financial support also was granted from the Ministerio de Ciencia y Tecnología (REN2001-4600-E).

References

Atkinson, R., Baulch, D.L., Cox, R.A., Crowley, J.N., Hampson, R.F.J., Hynes, R.G., Jenkin, M.E., Rossi, M.J., Troe, J.: Evaluated kinetic and photochemical data for atmospheric chemistry: Volume I – gas phase reactions of O_x, HO_x, NO_x and so_x species. Atmos. Chem. Phys. **4**, 1461–1738 (2004)

Becker, K.H.: EUPHORE: Final report to the European commission, EV5V-CT92-0059, Bergische Universität. Wuppertal, Germany (1996)

Bloss, C., Wagner, V., Bonzanini, A., Jenkin, M.E., Wirtz, K., Martin-Reviejo, M., Pilling, M.J.: Evaluation of detailed aromatic mechanisms (MCMv3 and MCMv3.1) against environmental chamber data. Atmos. Chem. Phys. **5**, 623–639 (2005)

Carter, W.P.L., Atkinson, R., Winer, A.M., Pitts, J.N.J.: Evidence for chamber-dependent radical sources: Impact on kinetic computer models for air pollution. Int. J. Chem. Kinet. **13**, 735–740 (1981)

Carter, W.P.L., Atkinson, R., Winer, A.M., Pitts, J.N.J.: Experimental investigation of chamber-dependent radical sources. Int. J. Chem. Kinet. **14**, 1071–1103 (1982)

Carter, W.P.L., Cocker, D.R., Fitz, D.R., Malkina, I.L., Bumiller, K., Sauer, C.G., Pisano, J.T., Bufalino, C., Song, C.: A new environmental chamber for evaluation of gas-phase chemical mechanisms and secondary aerosol formation. Atmos. Environ. **39**, 7768–7788 (2005)

Carter, W.P.L., Lurmann, F.W.: Evaluation of a detailed gas-phase atmospheric reaction-mechanism using environmental chamber data. Atmos. Environ. **25**, 2771–2806 (1991)

DeMore, W.B., Sander, S.P., Golden, D.M., Hampson, R.F.J., Kurylo, M.J., Howard, C.J., Ravishankara, A.R., Kolb, C.E., Molina, M.J.: Chemical kinetics and photochemical data for use in stratospheric modeling, Evaluation Number 12, JPL 97–4, Jet Propulsion Laboratory, Pasadena (1997)

Finlayson-Pitts, B.J., Wingen, L.M., Sumner, A.L., Syomin, D., Ramazan, K.A.: The heterogeneous hydrolysis of NO_2 in laboratory systems and in outdoor and indoor atmospehres: An integrated mechanism. Phys. Chem. Chem. Phys. **5**, 223–242 (2003)

Glasson, W.A., Dunker, A.M.: Investigation of background radical sources in a teflon-film irradiation chamber. Environ. Sci. Technol. **23**, 970–978 (1989)

Graham, R.A., Johnston, H.S.: Photochemistry of NO_3 and kinetics of N_2O_5-O_3 system. J. Phys. Chem. **82**, 254–268 (1978)

Heland, J., Kleffmann, J., Kurtenbach, R., Wiesen, P.: A new instrument to measure gaseous nitrous acid (HONO) in the atmosphere. Environ. Sci. Technol. **35**, 3207–3212 (2001)
Helton, J.C., Davis, F.J.: Latin hypercube sampling and the propagation of uncertainty in analyses of complex systems. SAND2001-0417, Sandia National Laboratories, Albuquerque, New Mexico (2002)
Jeffries, H.E., Sexton, K.G., Adelman, Z.: Auxiliary mechanism (wall models) for UNC outdoor chamber. Sixth US/Germany Workshop on Ozone/Fine Particle Science, pp 175–191
Killus, J.P., Whitten, G.Z.: Background reactivity in smog chambers. Int. J. Chem. Kinet. **22**, 547–575 (1990)
Kleffmann, J., Heland, J., Kurtenbach, R., Lörzer, J.C., Wiesen, P.: A new instrument (LOPAP) for the detection of nitrous acid (HONO). Environ. Sci. Pollut. Res. **9**, 48–54 (2002)
Madronich, S.: Troposperic ultraviolet-visible (TUV) radiation model, http://www.acd.ucar.edu/TUV/ (2003)
Madronich, S., Flocke, S.: The role of solar radiation in atmospheric chemistry, in P. Boule (ed.). Handbook of environmental chemistry, pp 1–26 (1998)
Pitts, J.N., Sanhueza, E., Atkinson, R., Carter, W.P.L., Winer, A.M., Harris, G.W., Plum, C.N.: An investigation of the dark formation of nitrous-acid in environmental chambers. Int. J. Chem. Kinet. **16**, 919–939 (1984)
Rivera-Figueroa, A.M., Sumner, A.L., Finlayson-Pitts, B.J.: Laboratory studies of potential mechanisms of renoxification of tropospheric nitric acid. Environ. Sci. Technol. **37**, 548–554 (2003)
Rohrer, F., Bohn, B., Brauers, T., Brüning, T., Johnen, F.-J., Wahner, A., Kleffmann, J.: Characterisation of the photolytic HONO-source in the atmosphere simulation chamber SAPHIR. Atmos. Chem. Phys. **5**, 2189–2201 (2005)
Rye, R.R., Martinez, R.J.: Photolithography of polytetrafluoroethylene for adhesion. J. Appl. Polym. Sci. **37**, 2529–2536 (1989)
Saltelli, A., Ratto, M., Tarantola, S., Campolongo, F.: Sensitivity analysis for chemical models. Chem. Rev. **105**, 2811–2827 (2005)
Saltelli, A., Scott, E.M., Chen, K.: Sensitivity analysis, Wiley, Chichester (2000)
Sander, S.P., Golden, D.M., Kurylo, M.J., Moortgat, G.K., Ravishankara, A.R., Kolb, C.E., Molina, M.J., Finlayson-Pitts, B.J.: Chemical kinetics and photochemical data for use in atmospheric studies. Evaluation Number 14, JPL 02-25, Jet Propulsion Laboratory, Pasadena (2002)
Saunders, S.M., Jenkin, M.E., Derwent, R.G., Pilling, M.J.: Protocol for the development of the master chemical mechanism, MCM v3 (part a): Tropospheric degradation of non-aromatic volatile organic compounds. Atmos. Chem. Phys. **3**, 161–180 (2003)
Turányi, T.: Sensitivity analysis of complex kinetic systems – tools and applications. J. Math. Chem. **5**, 203–248 (1990)
Turányi, T., Zalotai, L., Dóbé, S., Bérces, T.: Effect of the uncertainty of kinetic and thermodynamic data on methane flame simulation results. Phys. Chem. Chem. Phys. **4**, 2568–2578 (2002)
Zádor, J., Wagner, V., Wirtz, K., Pilling, M.J.: Quantitative assessment of uncertainties for a model of tropospheric ethene oxidation using the European photoreactor (EUPHORE). Atmos. Environ. **39**, 2805–2817 (2005)
Zádor, J., Zsély, I.G., Turányi, T., Ratto, M., Tarantola, S., Saltelli, A.: Local and global uncertainty analysis of a methane flame model. J. Phys. Chem. A **109**, 9795–9807 (2005)
Zhou, X.L., He, Y., Huang, G., Thornberry, T.D., Carroll, M.A., Bertman, S.B.: Photochemical production of nitrous acid on glass sample manifold surface. Geophys. Res. Lett. **29**, art. No. 1681 (2002)